Two-Dimensional Simulations of Coherent Fluctuation-Driven Transport in a Hall Thruster

IEPC-2013-212

Cheryl M. Lam[1] and Mark A. Cappelli, [2]
Stanford Plasma Physics Laboratory, Stanford University, Stanford, CA 94305, USA

and

Eduardo Fernandez[3]
Department of Mathematics and Physics, Eckerd College, St. Petersburg, FL, 33711, USA

Abstract: **This paper presents results and recent progress in two-dimensional hybrid fluid-PIC simulations of a Hall thruster. Motivated by experimental evidence of anomalously high electron mobility across the magnetic field that has been attributed to quasi-coherent fluctuations in the plasma properties, we use the numerical model to resolve azimuthal electron dynamics and study the impact of fluctuations on electron transport. As previously reported, the simulations predict some degree of enhanced transport beyond that due to classical scattering. As before, the simulations predict azimuthally-propagating disturbances. Of particular interest are recent simulations which predict a slow-moving rotating spoke-like disturbance near the thruster anode; while the spoke appears to generate current, it is not clear that the spoke results in anomalous electron transport.**

Nomenclatures

$\mu_\perp$	=	perpendicular electron mobility, based on classical scattering
v_{en}	=	electron-neutral collision frequency
ω_{ce}	=	electron cyclotron frequency
θ	=	azimuthal coordinate direction
$\boldsymbol{B}$	=	magnetic field vector
B_r	=	radial component of magnetic field
$D_\perp$	=	perpendicular diffusion constant, based on classical scattering
dt	=	time step
e	=	magnitude of electron charge, 1.6 x 10^{-19} C
$\boldsymbol{E}$	=	electric field vector
E_θ	=	azimuthal component of electric field
E_z	=	axial component of electric field
k	=	Boltzmann constant, 1.38 x 10^{-23} m^2 kg s^{-2} K^{-1}
n_e	=	electron number density

[1] Ph.D. Candidate, Mechanical Engineering Department, cheryl16@stanford.edu.
[2] Professor, Mechanical Engineering Department, cap@stanford.edu.
[3] Professor, Department of Mathematics and Physics, fernane@eckerd.edu.

1

$\vec{q}_e$	=	electron energy flux (heat flux)
r	=	radial coordinate direction
S_{ioniz}	=	electron energy loss due to ionization
S_{joule}	=	electron energy source term due to Joule heating
S_{wall}	=	electron energy loss due to wall collisions
t	=	time
T_e	=	electron temperature
$u_{e\theta}$	=	azimuthal electron velocity
u_{ez}	=	axial electron velocity
z	=	axial coordinate direction

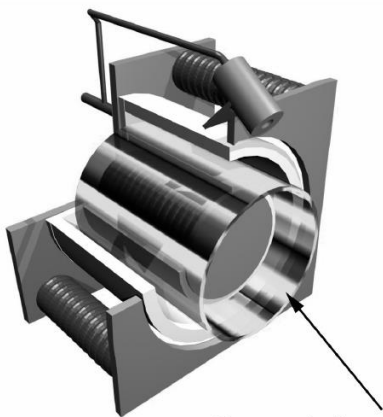# I.   Introduction

THE possibility of anomalously high electron mobility across the magnetic field has been experimentally documented since the early years of Hall thruster development.[1,2] The mechanism leading to this anomalous mobility remains as one of the key challenges in Hall thruster research. A lack of understanding of what generates anomalous mobility in some regions of the flow, while being very near classical in other regions, has curtailed the usefulness of certain two-dimensional (2D) hybrid simulations.[3-5]

Some theories attribute the anomalously high cross-field electron mobility to quasi-coherent fluctuations resulting from instabilities within the plasma.[1,4,6] There is also recent experimental evidence of coherent azimuthally-propagating fluctuations which may contribute to the observed enhanced cross-field transport.[2,7,8] Recently, there has been renewed interest in the rotating spoke phenomenon observed in the region of the Hall thruster channels nearest the anode, particularly the role that the spoke may play in contributing to enhanced electron transport upstream of the strong magnetic field region, and, ultimately, its impact on thruster performance and efficiency.

In this paper, we describe recent progress in using a two-dimensional hybrid fluid Particle-In-Cell model to resolve the electron dynamics in the azimuthal direction, i.e., in the axial-azimuthal (z-θ) plane. We report on recent advances and additions to the model, which have enabled quasi-steady simulations at a range of operating conditions. In particular, we have increased the axial grid resolution close to the anode, relative to simulations carried out previously,[9] so we can observe the possible development of strong disturbances in that region. We focus on understanding the role played by fluctuations, particularly those that propagate with components perpendicular to both the applied electric (E) and magnetic (B) field. We use the numerical model to characterize these oscillations and quantify their impact on the electron transport process, while making qualitative comparisons to experimentally-observed phenomena.

II.   Numerical Model

As previously reported, we have developed a two-dimensional axial-azimuthal (z-θ) model of a Hall thruster.[9] As far as we know, this was among the first z-θ-resolved simulations of an *entire thruster*, with the computational domain starting with the anode region and extending beyond the exit plane into the discharge plume, and including the full azimuth (0 to 2π radians). A schematic illustration of the thruster, indicating the simulated computational domain, is shown in Fig. 1.

The geometry simulated is that of a laboratory Hall discharge for which a considerable amount of experimental data has been gathered.[2,10] The discharge has an annular channel 8 cm in length and 1.2 cm in width, and an outer diameter of approximately 9 cm. The predominantly radial magnetic field peaks at a value of approximately B_r=.01 T just upstream of the channel exit.

The axial electric field is imposed by a positive voltage (relative to 0 V) applied at the anode. If we treat the

Computational Domain

Figure 1. Schematic of the thruster modeled and the computational domain.

2

magnetic field as purely radial, this gives an **E** x **B** drift velocity in the purely azimuthal direction. The model's 2D *z-θ* coordinate system is oriented such that the **E** x **B** drift velocity is in the positive *θ*-direction.

A. Model Description

The hybrid *z-θ* simulation tracks positive-ions and neutrals as discrete super particles, and treats the electrons as a fluid. The magnetic field is assumed to be in the radial direction, and we use the magnetic field measured in the SHT along the *z* axis at a midway radial location. The electron fluid is governed by continuity, momentum, and energy equations. The electron momentum is described by drift-diffusion and the model has two cross field electron velocity components, one in the axial direction, and the other in the azimuthal direction:

$$u_{e_z} = -\mu_\perp E_z - \frac{D_\perp}{n_e}\frac{\partial n_e}{\partial z} - \frac{D_\perp}{T_e}\frac{\partial T_e}{\partial z} - \frac{1}{1+\left(\dfrac{\nu_{en}}{\omega_{ce}}\right)^2}\frac{E_\theta}{B_r} - \frac{1}{1+\left(\dfrac{\nu_{en}}{\omega_{ce}}\right)^2}\frac{kT_e}{en_e B_r r}\frac{\partial n_e}{\partial \theta} \qquad 1.1$$

$$u_{e_\theta} = -\mu_\perp E_\theta - \frac{D_\perp}{n_e r}\frac{\partial n_e}{\partial \theta} + \frac{1}{1+\left(\dfrac{\nu_{en}}{\omega_{ce}}\right)^2}\frac{E_z}{B_r} + \frac{1}{1+\left(\dfrac{\nu_{en}}{\omega_{ce}}\right)^2}\frac{kT_e}{en_e B_r}\frac{\partial n_e}{\partial z} + \frac{1}{1+\left(\dfrac{\nu_{en}}{\omega_{ce}}\right)^2}\frac{k}{eB_r}\frac{\partial T_e}{\partial z} \qquad 1.2$$

To see how fluctuation-induced transport can occur, we note that the axial velocity has a fluctuating **E** x **B** term arising from azimuthal electric field perturbations. If the fluctuating plasma density is properly correlated with this fluctuating velocity, transport will result. We note that in the present version of the model, electron inertia terms are neglected.

Electron energy is described by a time-dependent equation:

$$\tfrac{3}{2}n_e k(\frac{\partial T_e}{\partial t} + \vec{u}_e \cdot \nabla T_e) + n_e k T_e \nabla \cdot \vec{u}_e - \nabla \cdot \vec{q}_e = S_{joule} - S_{ioniz} - S_{wall} \qquad 2$$

We include convective and diffusive fluxes, joule heating, ionization losses and an effective wall loss term. The electron energy equation is one-dimensional in *z*; the electron temperature is thus taken to be axisymmetric.

Neutral xenon atoms are treated as particles and are ionized according to the local ionization rate. The ionization rate depends nonlinearly on electron temperature; it is determined from fits using experimental cross sections and assuming a Maxwellian distribution assumption for the electrons. Neutral atoms are injected into the domain from the anode (*z* = 0) plane according to the prescribed mass flow rate. The neutral injection velocity is sampled from a half-Maxwellian distribution corresponding to anode temperature of 1000 K.

The ions, also treated as particles, are assumed to be non-magnetized and respond only to the electrostatic electric field. We couple the ion and electron treatments via quasineutrality; we calculate the plasma number density per the ion Particle-In-Cell (PIC) treatment and use this PIC value for the electron fluid equations.

Overall, we use a Finite Difference discretization scheme. The time-dependent electron temperature equation is solved via a fourth-order Runge-Kutta method. The electric field is not solved from Poisson's equation (since quasineutrality is assumed) and, instead, is obtained from combining the continuity and momentum equations and setting $n_e = n_i$. The heavy neutral and ion particles are advanced using a leap frog method with the ions subject to the interpolated electric field.

The same time step is used to advance both the particle motion and the electron fluid equations. At each step, neutrals are injected at the anode based on the mass flow rate. Neutrals are also ionized at each step according to the local ionization rate. This sequence of steps is repeated after a steady-state for the mean quantities is obtained. The steady-state is non-stationary; sustained electric current discharge oscillations are a distinctive feature of the simulation.

The electric potential is obtained by solving a convection-diffusion equation that results from combining the current continuity and momentum equations. The difficulty with this equation is the strong convection imposed by the electron **E** x **B** flow. We use a high-order upwind discretization method[11] in order to circumvent numerical instability. Such discretization results in a block-tridiagonal matrix for the electric potential that is solved via a direct-solve method. The boundary conditions are periodic in the azimuthal direction; for the axial direction, we impose axisymmetric (constant in *θ*) Dirichlet boundary conditions at the axial domain boundaries. While the

Dirichlet boundary condition at the anode is reasonable (the anode is at a fixed voltage), the downstream boundary condition is less clear; presently, the electric potential is set equal to that measured experimentally at the downstream domain boundary (0.04 m past the channel exit).

B. Recent Progress

Previous versions of this model neglected any radial physics, including wall collisions. In order to simulate a more realistic neutral density profile, we now use an ad-hoc method to model effective particle collisions at the inner and outer radius walls of the thruster channel. Each neutral or ion particle has an effective radial velocity and position which are time-advanced with the other (z and θ) velocity and position coordinates. Based on the particle's radial position, a wall collision is modeled. In the case of neutrals, particles are reflected upon collision with the anode plane or the channel inner and outer radial walls. Ions which strike the channel walls undergo recombination with an emitted donor electron to form a neutral. The particles are otherwise collisionless in that we do not model particle-to-particle collisions. Whereas previous simulations were stable only for low-voltage (~100V) thruster operating conditions, the inclusion of neutral reflection and ion recombination at the channel walls has enabled simulations at higher voltages (presently, up to 170V) which provide additional comparison points for laboratory experiments.

Due to renewed interest in capturing the rotating spoke phenomenon near the anode, we have explored using various grids which resolve the z-direction more finely. For these simulations, we often use a coarser grid in θ to reduce computational cost. Although there is some concern that the coarser azimuthal (θ) grid may not properly resolve fine spatial structure (i.e., high wave number fluctuations) in θ, for the case of the near anode spoke-like disturbance, the coarser azimuthal grid does not appear to significantly impact the predicted wave structure.

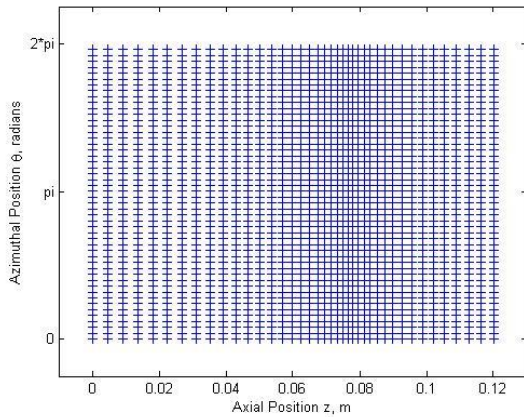## C. Discussion of Model Stability and Sensitivities

There remain a number of challenges in developing a robust simulation of sustained quasi-steady thruster operation. The model appears to be extremely sensitive to initial and boundary conditions. Depending on the choice of initial neutral and ion particle populations and distributions, the simulation may quickly become numerically unstable, while, in other cases, it will predict quasi-steady operation. The model is also highly sensitive to the initial electron temperature profile and the imposed Dirichlet boundary conditions for the electron energy equation. More generally, strong fluctuations in the electron temperature often drive the simulations into an unstable condition. We expect we may need to refine the electron energy equation, particularly the source and sink terms (right hand side of Eq. 2) such as the ionization cost and wall collision loss which are crudely modeled at present. Alternate boundary conditions might also give electron temperature and plasma density profiles that more closely resemble those observed in experiment.

Another concern is the lack of an enforced current conservation condition due to the finite difference discretization scheme. While we may be able to mitigate this effect with increased grid resolution, especially for high current regions, a finite volume scheme may be considered to assure current conservation.
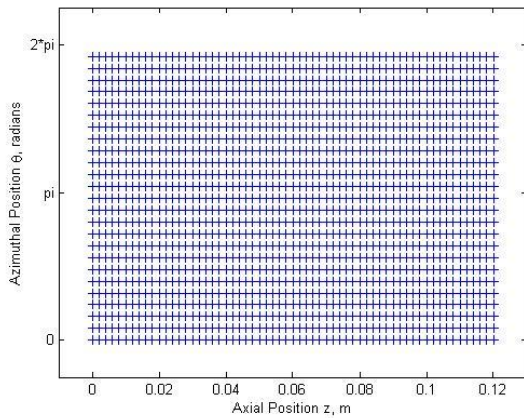
III.   Results

Simulations were performed for the described SHT geometry. A neutral mass flow rate of 2 mg/s was imposed to approximately match experimental operating conditions. A range of voltage operating conditions, between 100 V and 170 V, were simulated. Certain features of the simulated discharge, particularly the near anode behavior, were consistent across the simulations at various operating voltages. Here, we present results for the 100V operating condition; we compare these results to previous simulations results and experimental measurements for the same operating conditions.

The initial neutral population was established by first simulating a neutral only flow through the thruster channel; neutrals were injected at the anode and allowed to move through the computational domain, undergoing reflection at the walls as incident, until a stable neutral density profile developed. The ion population was initialized by assigning a uniform number of ion particles to each cell, with the ion particles randomly distributed in position within each cell; the ion velocities were initialized by inverting a Maxwellian velocity distribution. The initial electron temperature profile was interpolated based on the experimentally-measured profile; the anode and downstream electron temperature boundary conditions of 3.2 eV and 3.0 eV, respectively, were similarly inferred from experimental measurements. Throughout the simulation, the initial experimental-based electron temperature was periodically imposed to prevent the simulation from becoming unstable due to strong transient fluctuations in the electron temperature.

4

a) Previous simulation.

b) Present simulation.

Figure 2. Comparison of numerical grid resolution.

The major difference between the new simulations shown here and previous simulations is the grid resolution, as shown in Fig. 2. For the new simulations, we use a grid of 61 points uniformly spaced in z (Δz = 0.002 m) and 25 points uniformly spaced in θ ($\Delta\theta$ = 0.251 radians). Compared to previous simulations which used a non-uniform grid of 40 points in z and 50 points uniformly spaced in θ, the new simulations provide much finer axial grid resolution near the anode. As mentioned above, the new simulations also include the neutral collisions and ion recombination at the thruster walls which were not previously modeled.
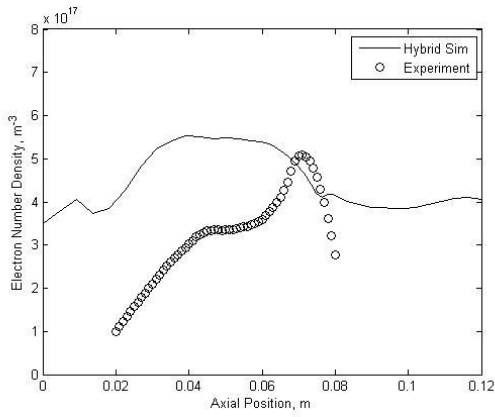
As a benchmark on establishing the computational cost for a typical run, a 180 μs simulation was performed using a timestep of 1 ns. The simulation took approximately 1 week to complete on a single Intel Xeon x5355 2.66GHz processor core; however, simulation (wall clock) time can be reduced by reducing the number of super particles simulated.
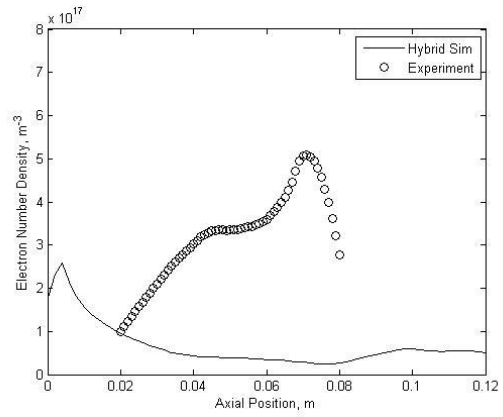
A. General Results

Figure 3 shows the time-averaged axial profiles of various plasma properties: electron number density (or plasma density), electric potential, electron temperature, and axial ion velocity. For the new simulation, the time average was taken over the time duration 90 μs to 170 μs; prior to 90 μs, start-up transients appear to dominate the simulation and the wave fluctuations have not yet stabilized. For both the present and previous simulations, the simulated time-averaged axial electrical potential and electron temperature profiles show good qualitative and order of magnitude agreement with experimental measurements. For the new simulation, the axial ion velocity shows an increasing trend (increasing axial velocity with increasing axial position) similar to experimental measurements inside the thruster channel ($z < 0.08$ m); however, downstream of the thruster exit plane, there is a sharp drop in the average axial ion velocity.
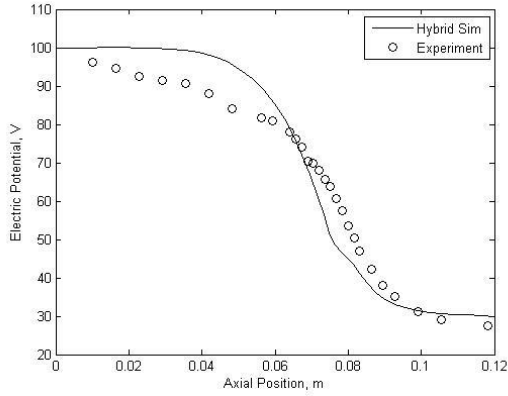
Note that in the new simulation, the electron number density is significantly lower than both experimental measurement and the previous simulation results. While the discrepancy between the present and previous simulations could be due to differences in the initial conditions, the new simulated electron density is an order of magnitude lower than the experimental measurements. The new axial profile is fairly constant with z, with the exception of a peak near the anode, and does not include the expected mid-channel peak shown in both experimental measurements and the previous simulation. Near the anode, the peak in the electron density starts to grow significantly toward the end of the simulation, eventually causing the simulation to become unstable. Figure 4 shows the electron number density profile for different times throughout the run; note the significant growth of the peak between $t = 160$ μs and $t = 170$ μs.
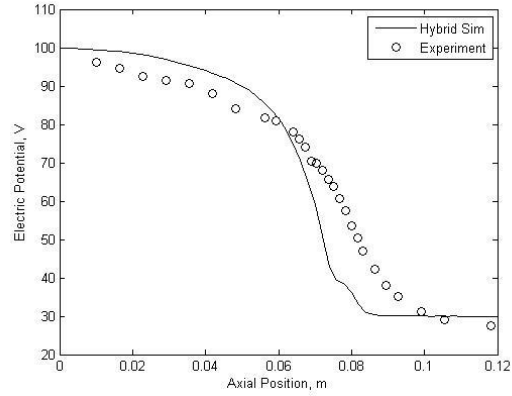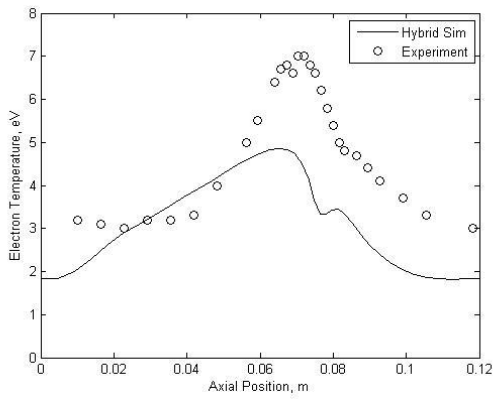
5

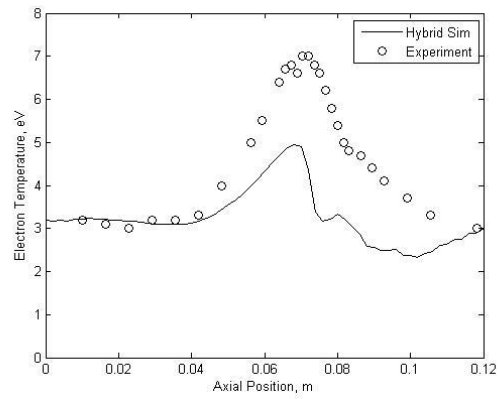**a) Electron number density.**

e) Electron number density.

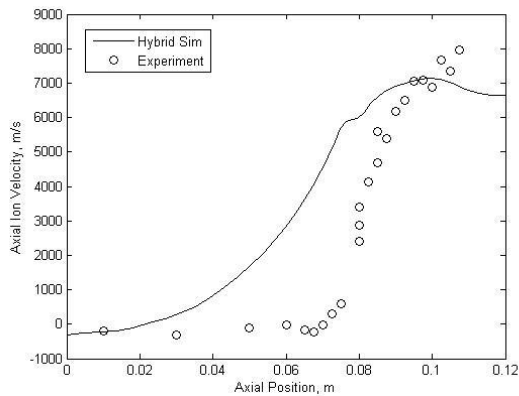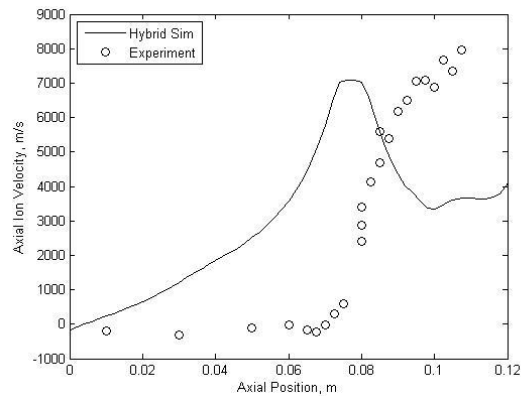**b) Electric potential.**

f) Electric potential.

c) Electron temperature.

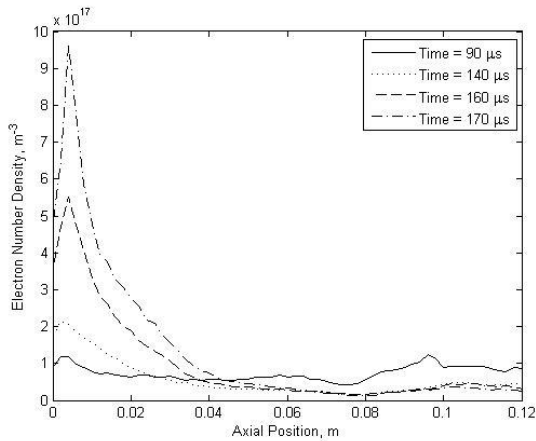**g) Electron temperature.**

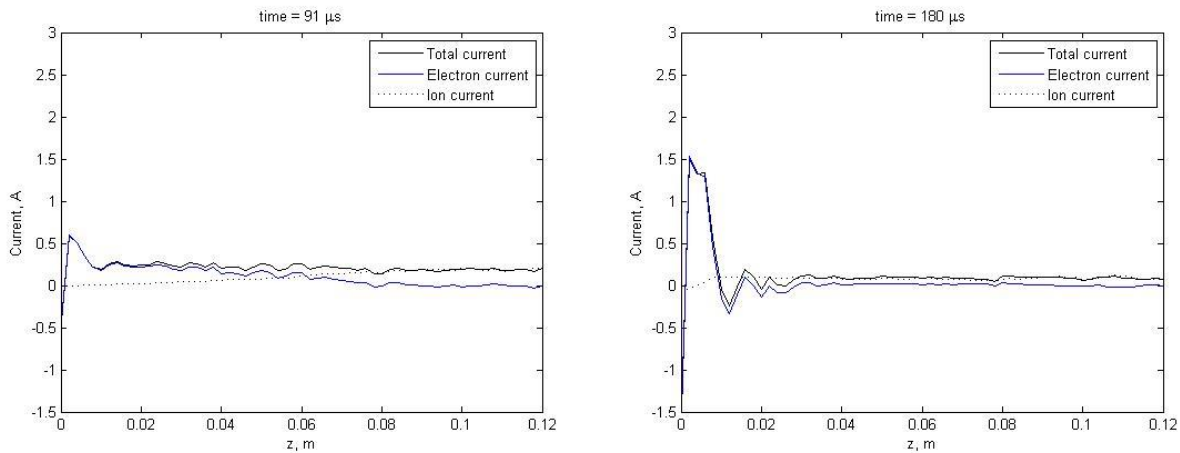**d) Axial ion velocity.**

h) Axial ion velocity.

Figure 3.   Comparison of time-averaged axial profiles for various plasma properties: a-d are for the previous simulation, e-h are for the present simulation.

Figure 4. Ionization near the anode leads to a peak in the electron number density.

The new simulation also predicts an extremely low discharge current which decreases with time. If we exclude the current due to the unstable growth of the plasma density peak near the anode, the simulated discharge current has a maximum value of approximately 0.5 A near the beginning of the simulation and decreases to values less than 0.1 A as the simulation continues; in experiments at this operating voltage, the measured discharge current was approximately 2 A. Figure 5 shows the axial current profile (summed over all θ for each axial position) for different times in the simulation; note that the total current varies with axial position, especially near the anode, indicating that the axial current is not conserved throughout the domain.
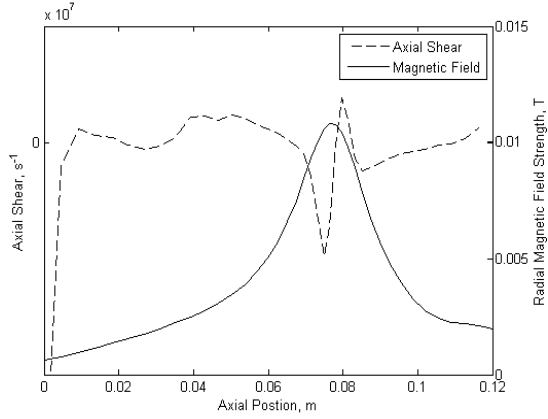

a) At time t = 91 μs.

b) At time t = 180 μs.

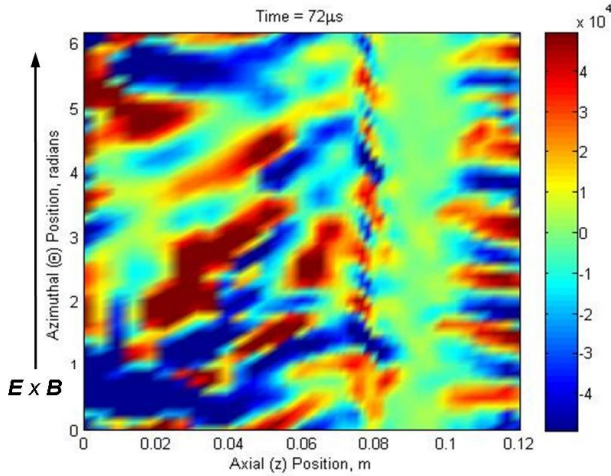**Figure 5. Snapshots of the election, ion, and total currents for different times in the simulation.**

B. Wave Propagation

As in the previous simulation, we observe dispersive tilted waves which propagate simultaneously in the axial and azimuthal directions. The new simulation predicts much of the same wave structure observed in the previous simulation (albeit with less spatial resolution in θ). Representative time snapshots of the axial electron velocity for both the present and previous simulation, shown in Fig. 6, illustrate the spatial wave structure and variation of wave properties with axial position. Although not shown here, we observe similar wave structure, with axial position, in the plasma density, electric potential, and azimuthal electron velocity.
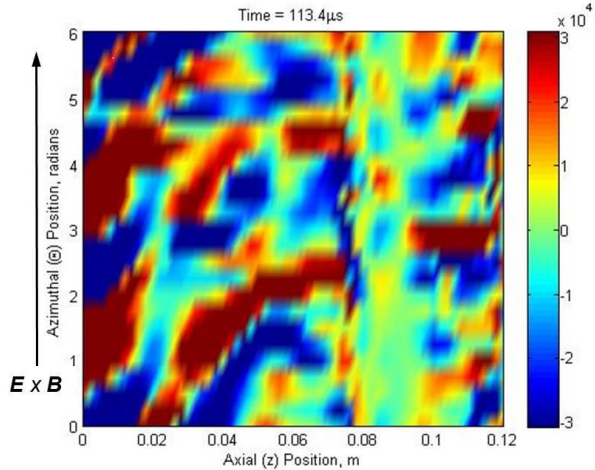
As in the previous simulation, we observe higher frequency, tilted waves, traveling in the positive z- and negative θ-directions, just upstream of the thruster channel exit plane (in the region approximately, 0.07 m ≤ z ≤ 0.08 m). As in the previous simulation, these waves have a shorter azimuthal wavelength and appear to advect out of the thruster channel, becoming purely axial (standing azimuthal waves) near z = 0.1 m with the same preserved azimuthal spatial structure. Further upstream, we observed lower frequency, longer wavelength waves in the region 0.02 m ≤ z ≤ 0.06 m; compared to the previous simulation, the wave structure in this region appear to be more tilted, i.e., there is appears to be a stronger, faster moving azimuthal component. As in the previous simulation, these waves appear to move towards the anode in the negative z-direction. Near the anode, the new simulations predict a slow moving tilted disturbance not observed in the previous simulations; we believe this structure to be consistent with the rotating spoke phenomena that has been predicted and observed near the anode.[1,8,12-14]

7

a) Variation of radial magnetic field strength B_r and axial shear $\partial u_{e\theta}/\partial z$ with axial position.

b) Previous simulation: representative time snapshot of axial electron velocity v_{ez}, at time t = 72 µs.

c) Present simulation: representative time snapshot of axial electron velocity v_{ez}, at time t = 113.4 µs.

Figure 6. Representative time snapshots of the axial electron velocity illustrate the spatial structure of wave propagation, with the axial magnetic field strength and shear shown for reference.

C. Rotating Spoke

Near the anode, in the region approximately $z < 0.2$ m, we observe a slow moving tilted disturbance propagating primarily in the $+ \mathbf{E} \times \mathbf{B}$ direction. The spatial wave structure indicates a $m = 2$ fluctuation with a primarily azimuthal phase velocity on the order of 1 km/s and frequency of approximately 10-20 kHz. The streak plot shown in Fig. 7 illustrates the azimuthal propagation of this disturbance; the observed spatial structure, velocity, and axial position are consistent with a rotating spoke near the anode.

In Fig. 5, we see that the axial current is highest in the region near the anode, which could be due to the current carried by the rotating spoke. We observe that the electron number density and axial electron velocity are strongly correlated in this region as shown in Fig. 8a; these correlated fluctuations in the electron density and velocity will generate electron current. By contrast, Fig. 8b shows a typical point further downstream within the thruster channel where the electron density and axial electron velocity are uncorrelated. Note that Fig. 8a shows the time history at a single (z, θ) point; to quantify the total electron current we must consider contributions across all θ.
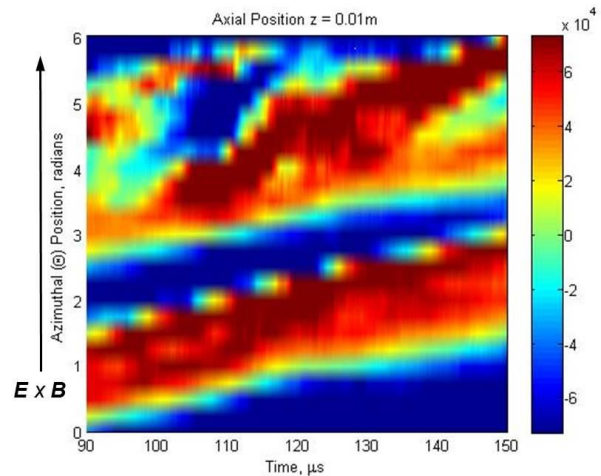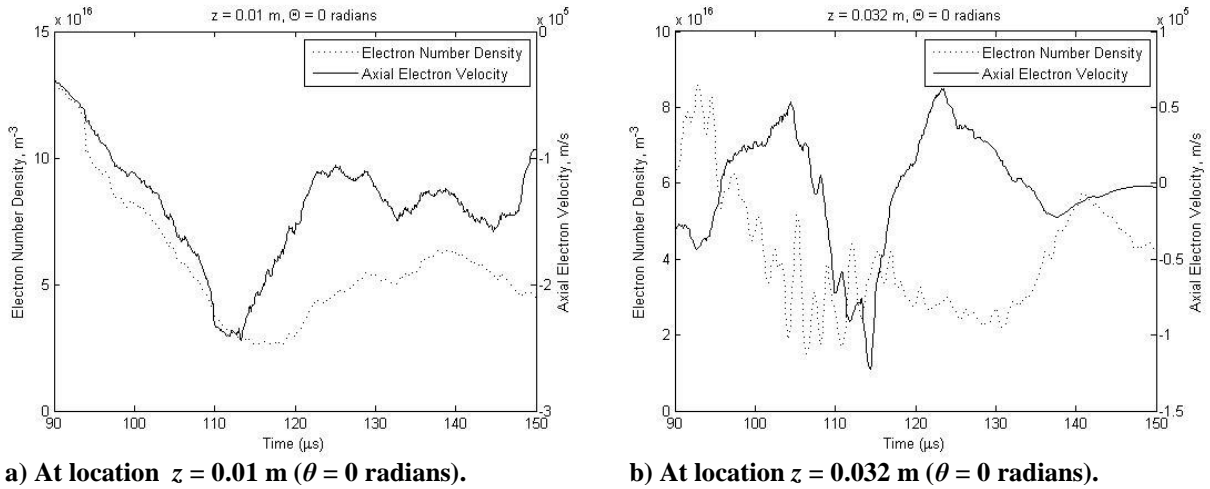

Figure 7. Present simulation: axial electron velocity streak plot at axial location $z = 0.01$ m, shown over the simulation time interval $t = 90-150$ µs.
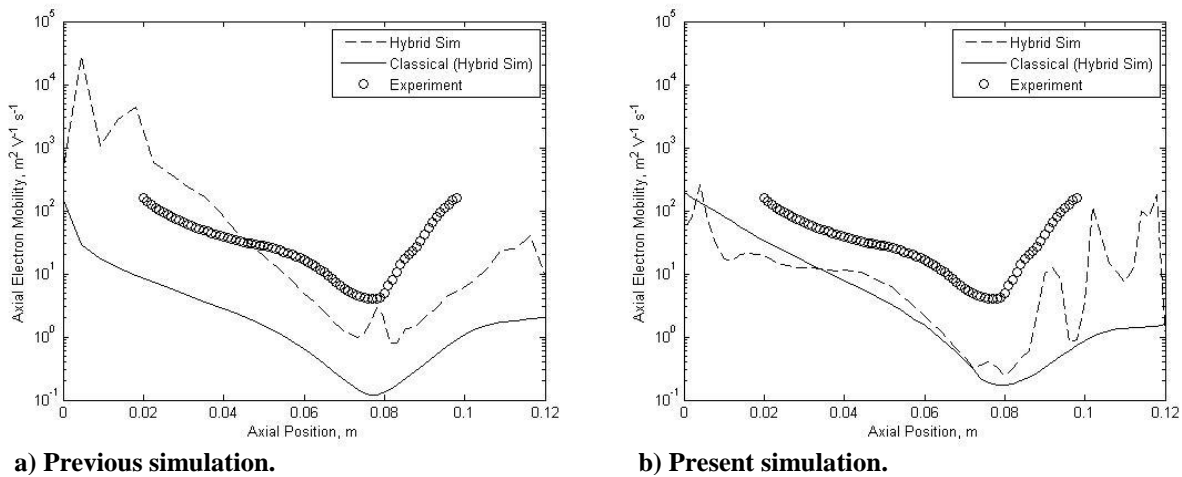
8

a) At location $z = 0.01$ m ($\theta = 0$ radians).   **b) At location $z = 0.032$ m ($\theta = 0$ radians).**

Figure 8. Time history of the electron number density and axial electron velocity over the time interval $t =$ 90-150μs at different axial locations.

D. Electron Transport

Overall, we are interested in the impact of azimuthal fluctuations on axial electron transport. Experimental measurements indicate an axial electron mobility significantly higher than that predicted by classical theory. It has been proposed that correlated fluctuations in the plasma density and electron velocity can enhance the axial electron mobility. In Fig. 9, we compare the axial electron mobility, predicted by the present and previous simulations; in each case, the classical mobility (based on simulated neutral number density and electron temperature) is shown for reference.

Despite the observation of correlated fluctuations in the electron density and electron velocity and higher current near the anode, the rotating spoke does not appear to generate anomalous transport. While the electron mobility is somewhat enhanced, compared to classical, in certain regions, the electron mobility is actually less than classical near the anode. Overall, the new simulation does not predict significant anomalous transport within the thruster channel. While the new simulation predicts a lower electron mobility in most regions, when compared to the previous simulation, this discrepancy could be due to the difference in plasma density magnitudes; the new simulation has a much lower plasma density throughout the thruster channel.

a) Previous simulation.   **b) Present simulation.**

Figure 9. Comparison of predicted electron axial mobility, as compared to experimentally-measured and classically-predicted values.

9

IV.   Conclusion

With increased axial resolution near the anode and other recent additions to the model, the axial-azimuthal hybrid simulation generates conditions which lead to the development of an observed rotating spoke. The simulated spoke characteristics (axial location, spatial structure, and velocity) are similar to those observed in several Hall thruster experiments. However in spite of increased current in the spoke region, based on preliminary simulations, the spoke does not appear to be responsible for anomalous transport upstream of the peak region of the magnetic field.

In general, the simulated plasma density and discharge current are low (compared to experiment). It appears that we have not effectively ignited the discharge and there may be a plasma cooling or quenching effect especially for simulations at lower operating voltages. To effectively simulate quasi-steady thruster operation we may need to artificially enhance the electron mobility using an alternate or additional electron mobility model. More generally, we continue to encounter challenges in maintaining numerical stability. We expect that refinements to the model will be needed to enable longer computationally-efficient simulations of quasi-steady thruster operation.

Acknowledgments

References

[1]Janes, G. S. and Lowder, R. S., "Anomalous Electron Diffusion and Ion Acceleration in a Low-Density Plasma," *Phys. Fluids **9***, 1115, 1966.

[2]Meezan, N. B., Hargus, W.A., Jr., and Cappelli, M. A., "Anomalous electron mobility in a coaxial Hall discharge plasma," *Physical Review*, Vol. 63, No. 2, 026410, 2001.

[3]Fernandez, E., Cappelli, M. A., and Mahesh, K., "2D simulations of Hall thrusters," *Center for Turbulence Research Annual Research Briefs*, Stanford Univ., Stanford, CA. 1998, pp.81-90.

[4]Fife, J. M., "Hybrid-PIC modeling and electrostatic probe survey of Hall thrusters," Ph.D. Dissertation, Dept. of Aeronautics and Astronautics, Massachusetts Inst. of Technology, Cambridge, MA, 1999.

[5]Hagelaar, G. J. M, Bareilles, J., Garrigues, L., and Boeuf, J. -P., "Two-dimensional model of a stationary plasma thruster," *J. Appl. Phys.*, Vol. 91, No. 9, 5592, 2002.

[6]Yoshikawa, S. and Rose, D. J., "Anomalous Diffusion of Plasma across a Magnetic Field," *Physics of Fluids*, Vol. 5, No. 3, 334, 1962.

[7]Knoll, A. K., "Plasma Oscillations and Associated Electron Transport within Hall Thrusters," Ph.D. Dissertation, Department of Mechanical Engineering, Stanford University, Stanford, CA, 2010.

[8]Ellison, C. L., Raitses, Y., and Fisch, N. J., "Cross-field electron transport induced by a rotating spoke in a cylindrical Hall thruster," *Phys. Plasmas*, Vol. 19, No. 1, 013503, 2012.

[9]Lam, C. M., Knoll, A.K., Cappelli, M. A., and Fernandez, E., "Two-Dimensional (z-θ) Simulations of Hall Thruster Anomalous Transport," *International Electric Propulsion Conference*, Ann Arbor, MI, 2009, IEPC-2009-102.

[10]Hargus, W. A., "Investigation of the plasma acceleration mechanism within a coaxial Hall thruster," Ph.D. Disseration, Mechanical Engineering Dept., Stanford Univ., Stanford, CA, 2001.

[11]Fletcher, C. A. J., *Computational Techniques for Fluid Dynamics 1*, 2nd ed., Springer-Verlag, New York, 1991.

[12]Chesta, E., Lam, C. M., Meezan, N. B., Schmidt, D. P., and Cappelli, M. A., "A Characterization of plasma fluctuations within a Hall Discharge," *IEEE Transactions on Plasma Science*, Vol. 29., No. 4, 2012.

[13]Gascon, N. and Cappelli, M.A., "Wall Effects on the Excitation and Propagation of Instabilities in Hall Thrusters," *International Electric Propulsion Conference*, 2003, IEPC-2003-0328.

[14]Chouieri, E., "Plasma oscillations in Hall thrusters," *Phys. Plasmas **8***, 1411, 2001.

The 33st International Electric Propulsion Conference, The George Washington University, USA
October 6 – 10, 2013